Tuning the Dzyaloshinskii-Moriya interaction in Pt/Co/MgO heterostructures through the MgO thickness

Nanoscale

PAPER

View Article Online
View Journal | View Issue

Cite this: *Nanoscale*, 2018, **10**, 12062

Tuning the Dzyaloshinskii–Moriya interaction in Pt/Co/MgO heterostructures through the MgO thickness†

Anni Cao, ‡[a] Xueying Zhang, ‡[a,b,c] Bert Koopmans,[d] Shouzhong Peng,[a] Yu Zhang,[a,b] Zilu Wang,[a] Shaohua Yan,[a] Hongxin Yang[e] and Weisheng Zhao *[a,c]

Received 30th October 2017,
Accepted 22nd May 2018

DOI: 10.1039/c7nr08085a

rsc.li/nanoscale

The interfacial Dzyaloshinskii–Moriya interaction (DMI) in ferromagnetic/heavy metal ultra-thin film structures has attracted a lot of attention thanks to its capability to stabilize Néel-type domain walls (DWs) and magnetic skyrmions for the realization of non-volatile memory and logic devices. In this study, we demonstrate that magnetic properties in perpendicularly magnetized Ta/Pt/Co/MgO/Pt heterostructures, such as magnetization and DMI, can be significantly influenced by the MgO thickness. To avoid the excessive oxidation of Co, an ultrathin Mg layer is inserted to improve the quality of the Co–MgO interface. By using field-driven domain wall expansion in the creep regime, we find that non-monotonic tendencies of the DMI field appear when changing the thickness of MgO. With the insertion of a monatomic Mg layer, the strength of the DMI could reach a high level and saturate. We conjecture that the efficient control of the DMI is a result of subtle changes of both Pt/Co and Co/MgO interfaces, which provides a method to optimize the design of ultra-thin structures achieving skyrmion electronics.

Introduction

In the past few years, the Dzyaloshinskii–Moriya Interaction (DMI) has attracted significant interest[1] because it is one of the key ingredients in the creation of magnetic skyrmions and chiral domain walls (DWs), which are promising for the next generation of high-speed magnetic storage devices. After more than two decades of theoretical studies,[2–4] magnetic skyrmions were first observed at low temperatures in hexagonal lattices in non-centrosymmetric crystals[5–7] and magnetic multilayers.[8–10] On the other hand, the interfacial DMI induced by symmetry breaking at the interface appears to be particularly important. In addition, DW motion close to 1000 m s^{-1} has been observed[11] The polarized spin current from the heavy metal layer due to the spin Hall effect combined with a Néel-type DW configuration[12–14] stabilized by the strong DMI can be used to explain such a fast motion. Although some experimental efforts have been recently devoted to quantifying the DMI and the underlying physics, the mechanism of interfacial DMI is still elusive. Nevertheless, enhancement of DMI can be achieved by fine tuning of the interface configuration.[15–17] Therefore, effective control of DMI is essential in developing advanced storage class memory devices.[18]

In this paper, we propose a method to control the DMI by changing the thickness of the MgO layer in a Pt/Co/oxide system. The thickness of MgO of samples was tuned *via* a wedge structure and the corresponding effective DMI field was quantified by searching for its compensating in-plane field that minimized the DW motion velocity in the creep regime. Samples with 0.2 nm Mg inserted between Co and MgO have also been prepared. We found that the variation of the effective DMI field can be attributed to the details of the Pt/Co interface, which indicates that the influence on the adjacent interfaces of MgO could be used to regulate the interfacial DMI thanks to large charge transfer and the interfacial electric field.[19] We also unveiled that the insertion of monoatomic Mg can help in the tuning of the DMI through the MgO layer and to get a great value of up to 2.32 mJ m^{-2}.

Sample preparation

Samples with the structure of Ta(3 nm)/Pt(3 nm)/Co(1 nm)/MgO(t)/Pt(5 nm) and Ta(3 nm)/Pt(3 nm)/Co(1 nm)/Mg

[a]*Fert Beijing Institute, BDBC, School of Electronic and Information Engineering, Beihang University, Beijing, China. E-mail: weisheng.zhao@buaa.edu.cn*
[b]*Centre for Nanoscience and Nanotechnology, University Paris-Saclay, Orsay, France*
[c]*Beihang-Goertek Joint Microelectronics Institute, Qingdao Research Institute, Beihang University, Qingdao, China*
[d]*Department of Applied Physics, Institute for Photonic Integration, Eindhoven University of Technology, Eindhoven, The Netherlands*
[e]*Key Laboratory of Magnetic Materials and Devices, Ningbo Institute of Materials Technology and Engineering, Chinese Academy of Sciences, Ningbo, Zhejiang, China*
†Electronic supplementary information (ESI) available: Additional experiment results of DW motion, and calculation of the demagnetizing field and stray field. See DOI: 10.1039/c7nr08085a
‡These authors contributed equally to this work.

(0.2 nm)/MgO(t)/Pt(5 nm) were firstly deposited on a 500 μm Si wafer with a 300 nm thermal oxide layer by magnetron sputtering at room temperature, as shown in Fig. 1. The (111) texture of the bottom Pt was ensured by a Ta seed layer,[20] while the top Pt performed as a protective layer preventing the film oxidation. The base pressure of our ultrahigh vacuum deposition system is around 3×10^{-8} mbar. In order to exclude the influence of variable growth conditions on the MgO quality, and thus to make the MgO thickness the only variable in our system, the MgO layer was designed in a wedge structure. The thickness of MgO (t_{MgO}), which has been calibrated using an atomic force microscope (AFM), varies from 0.40 nm to 1.26 nm in 8 cm length for the samples without a Mg layer, while t_{MgO} varies from 0.20 nm to 2.00 nm in the samples with a Mg insertion layer. In addition, a sample of the same structure without a MgO layer was prepared as a reference. A sectional view by Cs-corrected Transmission Electron Microscopy and X-ray energy dispersive spectroscopy (EDS) curves are shown in Fig. 1(a) and (b) for samples without and with the ultrathin Mg layer. As shown in Fig. 1(a), except for the amorphous Co and MgO, each layer can be distinguished clearly. In contrast, Fig. 1(b) shows a much better resolution, as particularly clear in the inset which shows the Pt/Co/Mg/MgO/Pt part of the structure with a larger scale. The crystalline structure of the Pt/Co interface for samples with Mg is superior compared to the other. Since the peaks of the EDS curves are indicative of the center of each layer, we can deduce that oxygen and magnesium permeated into the Co layer till some extend for both samples, but the insertion of a Mg layer separates cobalt and oxygen most effectively.

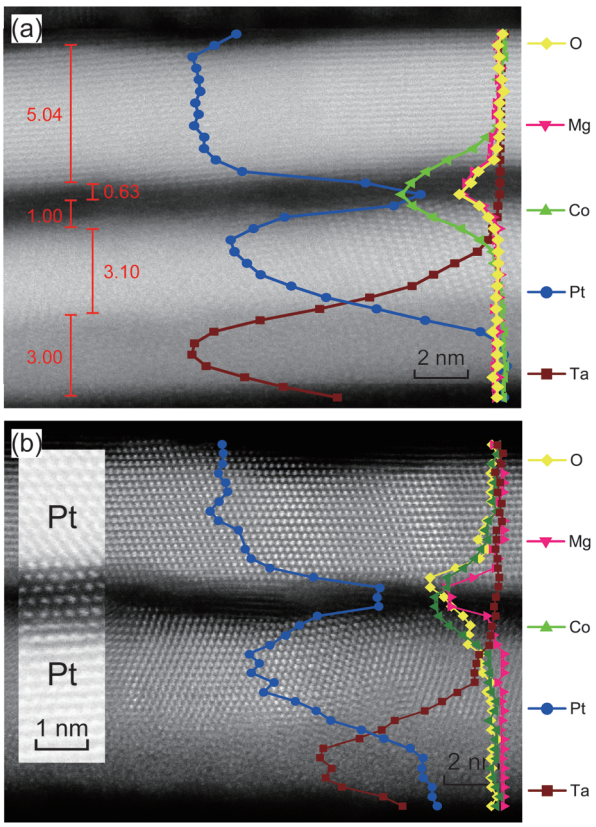

Fig. 1 Cross profile of the samples (a) without a Mg layer at $t_{MgO} \approx$ 0.60 nm and (b) with a Mg layer at $t_{MgO} \approx$ 0.80 nm as measured by transmission electron microscopy.

Measurements of magnetic properties

The wedge samples were cut into small squares with the lengths of the side equal to 2.5 mm for vibrating sample magnetometer (VSM) measurement. Fig. 2(a) and (b) show the hysteresis loops of two groups of samples with perpendicular magnetic fields at room temperature. It can be seen that all samples exhibit obvious perpendicular anisotropy. We can see that the saturation magnetization M_s and the coercive field H_c decrease with the increase of MgO thickness for the samples without Mg protection as shown in Fig. 2(c), while this decrease is avoided in the samples with an inserted Mg layer (Fig. 2(d)). The largest variation appears in the loops with the thinnest MgO and without MgO. The interfacial PMA can be calculated as $K_{eff} = \frac{1}{2}\mu_0 H_K M_s$, where K_{eff} is the effective magnetic anisotropy energy, and H_K is the effective anisotropy field[21,22] obtained by extracting the field corresponding to 90% of M_s in curves with an in-plane field. As shown in Fig. 2(c), the saturation magnetization M_s decreases by 75% as the MgO thickness increases from 0 to 1.26 nm, which is due to the partial oxidation of Co. Also, the proximity induced magnetic moment in Pt will be quenched after inserting the MgO barrier. As shown in Fig. 2(d), this significant shrinkage disappears when the Mg is inserted between Co and MgO. After insertion, the reduction of M_s is only about 20%. The effective anisotropy field H_K seems not to vary remarkably in both Fig. 2(c) and (d), so the trends of the effective magnetic anisotropy energy K_{eff} are attributed to the variation of M_s to some extent.

Characterization of the DMI

In order to quantify the DMI in the various samples, we studied the asymmetric DW motion in the creep regime when an in-plane field was applied. In a sample with PMA and a strong DMI, the magnetization in the center of DWs is fixed in a chiral direction by the effective DMI field H_{DMI}, *i.e.*, DW configurations are of Néel type. The presence of an in-plane field will break this configuration, thus affecting the surface energy of DWs. This change will further influence the field driven DW velocity in the creep regime. For a fixed perpendicular driving field, the minimal DW velocity occurs when H_{DMI} is completely compensated by the in-plane field. This compensating field can be seen as an indicator of the strength of the DMI and was widely used to quantify H_{DMI}.[23–25]

In our experiments, a Kerr microscope was used to measure the DW velocity. After saturating the sample, when an out of

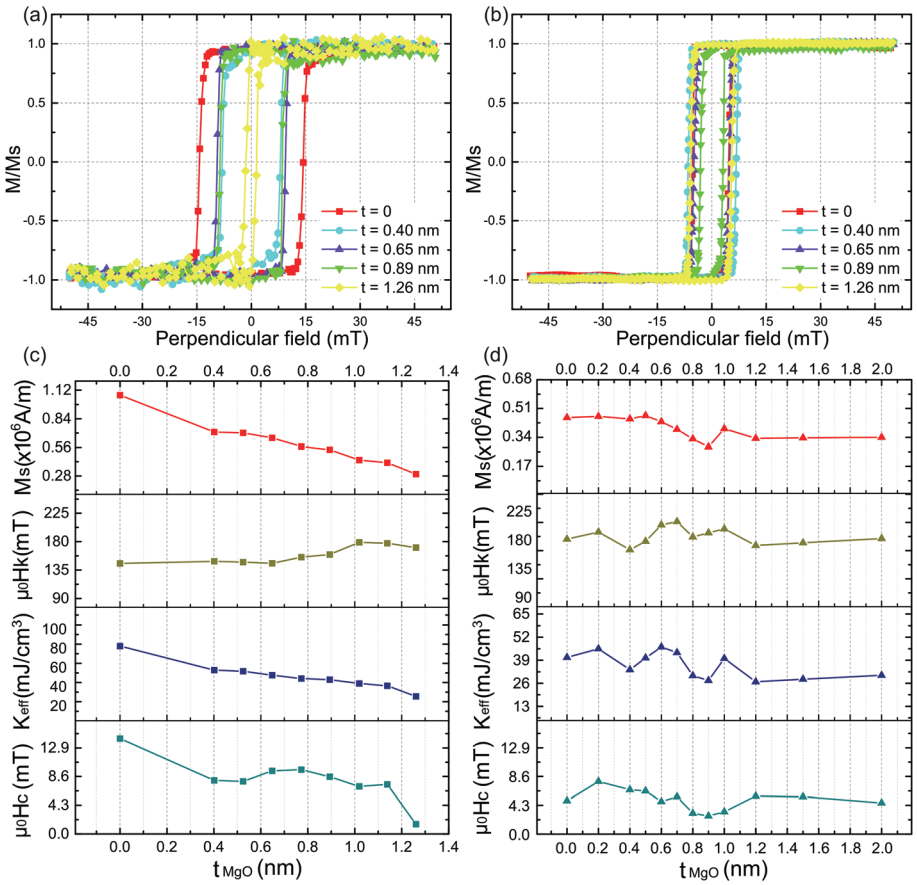

Fig. 2 Hysteresis loops with a perpendicular magnetic field for (a) the Ta/Pt/Co/MgO(t_{MgO})/Pt stacks and (b) the Ta/Pt/Co/Mg(0.2 nm)/MgO(t_{MgO})/Pt stacks with different MgO thicknesses. Magnetic properties obtained from the hysteresis loops for samples (c) without and (d) with a Mg insertion layer.

plane field $\mu_0 H_z$ was applied (~10 mT) in the opposite direction, domain bubbles will be nucleated and continuously expand. In creep mode, the DW expansion is not so fast (10^{-4}–10^{-5} m s^{-1}) so that we can capture Kerr images at a fixed time interval (0.08 s). Then the DW velocity can be calculated by analyzing this dynamic process. At the same time, an in-plane field H_x could be applied and the DW velocity variation caused by H_x could be probed, as shown in Fig. 3. Since the perpendicular component of H_x on the drive field H_z would exponentially influence the v (as shown in Fig. S1 and S2 in the ESI†), the sample was placed at the very center of the quadrupole magnet poles to avoid the probable interference with the measurement of velocity. In order to make sure that the applied in-plane field was exactly parallel to the sample and its stray field in perpendicular was negligible, we have checked that when H_z was removed, no DW motion would be seen even when the applied $\mu_0 H_x$ was increased to a relatively high value (~300 mT). Moreover, the leftmost velocity and rightmost velocity should exhibit symmetry about the x-axis. By performing DW motion measurement in this way, it was observed that as the thickness of the MgO layer grows, more intensive DWs caused by interfacial defect appear, which indirectly hint at the decrease of the coercive field H_c.

A selection of our DW velocity measurements is shown in Fig. 4. The dependence of the velocity on the in-plane field is found to be roughly quadratic, where the minimum occurs at a non-zero value of H_x. On reversing H_z, a very similar quadratic $H_x - v$ dependence is found, however, with a minimum occurring at the opposite value of H_x, as shown by black and red data points respectively. Similar $H_x - v$ measurements performed at different H_z values are shown in Fig. S3 in the ESI.† We have estimated the influence of the inhomogeneity of the demagnetizing field and the stray field on different zones of the sample and found that this influence is negligible, see ESI.† In order to exclude the direct influence of the thickness gradient on the DW motion velocity, we scaled the velocity at the same rightmost place of the same domain and measured the same DW motion direction. Moreover, all measurements were focused on a zone of about 1.6 × 1.6 mm^2. In such a small zone, the variation of the MgO thickness is less than 2×10^{-4} nm. So the velocity asymmetry caused by the structural gradient could be neglected. Therefore, we conclude that the velocity asymmetry shown in Fig. 4 is mainly induced by the DMI. Following the procedure in ref. 30, H_{DMI} is obtained from the in-plane field value corresponding to the lowest v, although we are aware of the problems of this method in certain cases.[26,27]

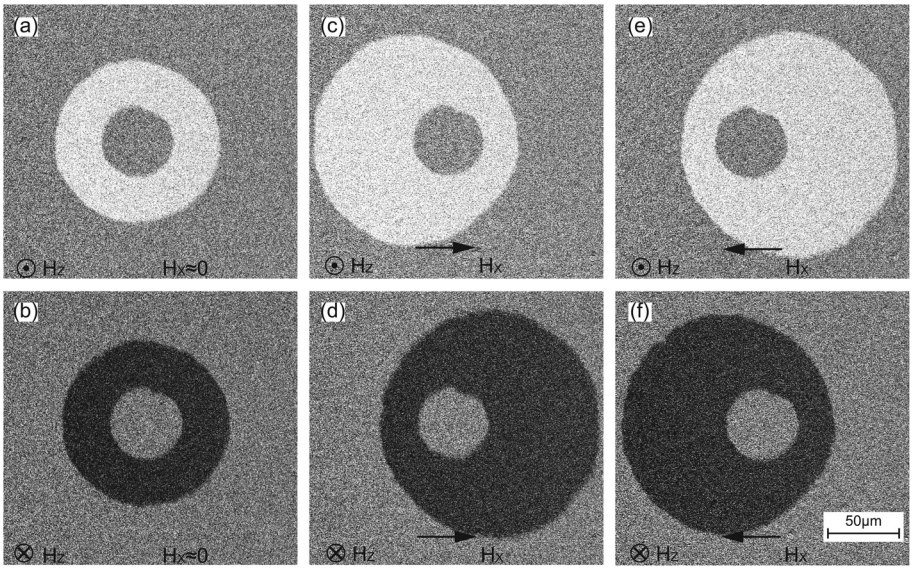

Fig. 3 DW expansion of Pt/Co/Mg/MgO(0.6 nm)multilayers driven by an out-of-plane magnetic field $\mu_0|H_z|$ = 8 mT. (a) (b) with an in-plane field $\mu_0 H_x$ approximately 0, (c)–(f) with $\mu_0|H_x|$ = 327 mT. Field directions have been marked in each image. Images in (a)–(f) were obtained by subtracting four images with a specific time interval from a background with no DW. All images of DW were captured using a Kerr microscope.

The trends of the effective DMI field are depicted in Fig. 5 with solid symbols. Since the $|H_{DMI}|$ of all samples with a MgO layer in our experiments are stronger than the samples without MgO, the insertion of MgO enhances the DMI, especially for those samples with Mg inserted between Co and MgO. It is also found that, for the samples without a Mg layer, the H_{DMI} first increases as a function of MgO thickness, and after an optimum around 0.7 nm it decreases again. In contrast, H_{DMI} for the samples with a Mg layer increases and saturates at a relatively high level. By assuming an exchange stiffness constant A = 15 pJ m^{-1} (ref. 28 and 29) and substituting the experimental results into $|H_{DMI}| = |D|/\left(\mu_0 M_s \sqrt{A/K_{eff}}\right)$,[30] the absolute value of the DMI constant $|D|$ exhibits a similar trend to $|H_{DMI}|$ in both groups of samples. The maximum $|D|$ value of 0.77 mJ m^{-2} occurs at the MgO thickness of 0.65 nm for the samples without monatomic Mg. Surprisingly, the $|D|$ reaches up to 2.32 mJ m^{-2} after the Mg was inserted between the Co/MgO interface. The saturated $|D|$ value of the samples with Mg is comparable to the published result of D = 2.05 mJ m^{-2} in the same structure.[31]

Discussion

Using the above method, we carried out our measurements of H_{DMI} *versus* MgO thickness on all samples with or without a Mg layer; the results are shown in Fig. 5. For Pt/Co/MgO samples, the strength of the DMI exhibit first an increasing and then a decreasing trend, whereas a stable stage following an escalating trend can be seen for Pt/Co/Mg/MgO samples. In addition, the highest values of both H_{DMI} and $|D|$ for the samples with Mg are almost 3 times greater than the peak value for the samples without Mg. However, here it is unexpected that when the MgO thickness is higher than the critical thickness, the DMI starts to decrease. On comparing the experimental results of the samples with a Mg insertion layer, it can be inferred that excessive oxidation is the main reason for the DMI reduction. When MgO grows thicker, the stabilization of the DMI for the samples with Mg is more likely to reveal that the tuning of the DMI is an interfacial effect.

As a primary dominant mechanism, upon inserting MgO, the structure is effectively changed from Pt/Co/Pt, which is nearly inversion symmetric and has a relatively weak DMI towards Pt/Co/MgO, which is a prototype asymmetric structure with a large DMI. As a consequence, the DMI shoots up after insertion of MgO. Secondly, further changes may be assigned to the interface between Co and Pt, and could involve several mechanisms. On the one hand, the oxidation of Co mentioned above decreases the effective Co thickness introducing the DMI with the Pt layer.[32] On the other hand, the lattice mismatch between Co and MgO may induce a strain effect on the Pt/Co interface[33,34] although the MgO layer is sputtered after the Co layer, MgO modifies the Pt/Co interface and influences the spin–orbit coupling (SOC) between the bottom Pt and Co. Last but the most important, as for the Co/MgO interface, according to density functional theory calculations, interfacial oxidation is related to large charge transfer and to the large interfacial electric field that compensates the small spin–orbital coupling of the atoms at the interface, directly increasing the DMI.[31,35] It has been calculated that, different from the Pt/Co interface, the DMI and SOC energy source of the Co/MgO interface are localized in the interfacial Co layer,[31,36] which indicates a diverse mechanism governed by the Rashba effect.[37–39]

Note that the influence of the DMI on the free layer and the performance of the device has been intensively studied in

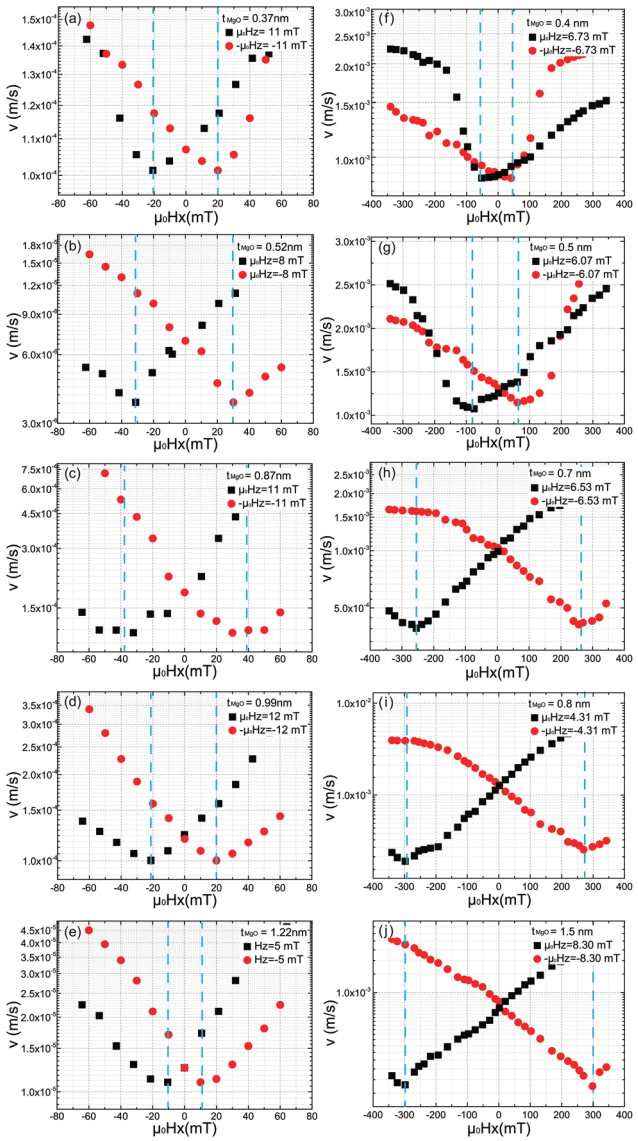

Fig. 4 (a)–(e) Rightmost DW velocities of Pt/Co/MgO samples with $\mu_0 H_x$ varying from −60 to 60 mT, (f)–(j) right-hand-edge DW velocities of Pt/Co/Mg/MgO samples with $\mu_0 H_x$ varying from −350 to 350 mT. Perpendicular fields ($\mu_0 H_z$) in both directions were measured. The blue vertical dashed lines stand for the place we got $\mu_0 H_{DMI}$.

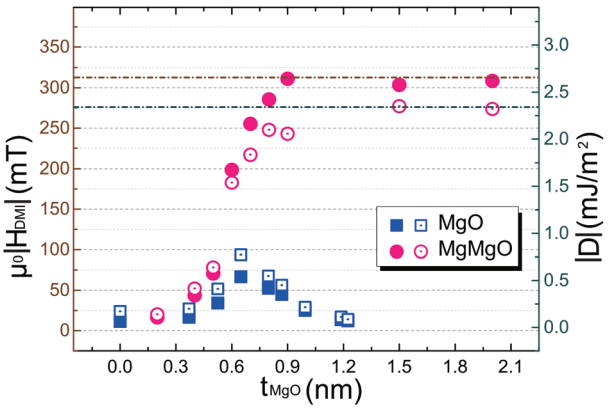

Fig. 5 Trends of the effective DMI field and DMI constant as a function of t_{MgO}. Square symbols stand for Pt/Co/MgO(t_{MgO}) samples while circular symbols stand for Pt/Co/Mg/MgO(t_{MgO}). Closed symbols stand for $\mu_0|H_{DMI}|$ and open symbols stand for $|D|$.

recent years.[40] In addition, some devices based on the skyrmionic state in the free layer of a MTJ were proposed.[41] The TMR was also a critical factor when we detect skyrmions using an effective electrical method.[42,43] As the HM/FM/MgO structure we studied is very similar to the configuration of the tunnel barrier layer/free layer/capping layer of the most popular MTJ structure,[44] our study could be therefore very useful to investigate the properties and effects of the DMI for the electrical nucleation and detection of magnetic skyrmions through MTJ. Not only Co, but also the influence of MgO on adjacent interfaces could be used to fine-tune the DMI in Pt/Co/MgO samples which is valuable for the induction of chiral magnetic order.

Conclusion

In conclusion, varying the thickness of MgO in a Pt/Co/MgO material system can significantly affect the Dzyaloshinskii–Moriya interaction. The DW motion was measured to characterize the strength of the DMI, which is caused by the structural asymmetry between the top interface and bottom interface. We found that indeed it is possible to tune the DMI by varying the MgO thickness, especially when Co is protected by an ultrathin Mg insertion layer. Not only the Co/MgO interface but also the Pt/Co interfaces were changed. This study will be very helpful for thin film design to obtain a large DMI and stabilize magnetic skyrmions with an expected size for memory and logic devices.

Conflicts of interest

There are no conflicts to declare.

Acknowledgements

The authors would like to acknowledge the support by the projects from the National Natural Science Foundation of China (No. 61571023, 61627813 and 61471015), the Beijing Municipal of Science and Technology (No. Z161100000216149), the International Collaboration Project from the Ministry of Science and Technology in China (No. 2015DFE12880), and the Program of Introducing Talents of Discipline to Universities in China (No. B16001).

References

1 B. Pang, L. Zhang, Y. B. Chen, J. Zhou, S. Yao, S. Zhang and Y. Chen, *ACS Appl. Mater. Interfaces*, 2017, **9**, 3201–3207.

2 B. A. Ivanov, V. A. Stephanovich and A. A. Zhmudskii, *J. Magn. Magn. Mater.*, 1990, **88**, 116–120.
3 A. Bocdanov and A. Hubert, *Phys. Status Solidi*, 1994, **186**, 527–543.
4 A. Abanov and V. L. Pokrovsky, *Phys. Rev. B: Condens. Matter Mater. Phys.*, 1998, **58**, 8889–8892.
5 S. Muhlbauer, B. Binz, C. Pfleiderer, A. Rosch, A. Neubauer, R. Georgii and P. Boni, *Science*, 2013, **323**, 915–919.
6 X. Z. Yu, Y. Onose, N. Kanazawa, J. H. Park, J. H. Han, Y. Matsui, N. Nagaosa and Y. Tokura, *Nature*, 2010, **465**, 901–904.
7 A. Tonomura, X. Yu, K. Yanagisawa, T. Matsuda, Y. Onose, N. Kanazawa, H. S. Park and Y. Tokura, *Nano Lett.*, 2012, **12**, 1673–1677.
8 H. Du, R. Che, L. Kong, X. Zhao, C. Jin, C. Wang, J. Yang, W. Ning, R. Li, C. Jin, X. Chen, J. Zang, Y. Zhang and M. Tian, *Nat. Commun.*, 2015, **6**, 8504.
9 D. A. Gilbert, B. B. Maranville, A. L. Balk, B. J. Kirby, P. Fischer, D. T. Pierce, J. Unguris, J. A. Borchers and K. Liu, *Nat. Commun.*, 2015, **6**, 8462.
10 W. Jiang, G. Chen, K. Liu, J. Zang, S. G. E. te Velthuis and A. Hoffmann, *Phys. Rep.*, 2017, **704**, 1–49.
11 S. Yang, K. Ryu and S. Parkin, *Nat. Nanotechnol.*, 2015, **10**, 221–226.
12 A. V. Khvalkovskiy, V. Cros, D. Apalkov, V. Nikitin, M. Krounbi, K. A. Zvezdin, A. Anane, J. Grollier and A. Fert, *Phys. Rev. B: Condens. Matter Mater. Phys.*, 2013, **87**, 20402.
13 S. M. Seo, K. W. Kim, J. Ryu, H. W. Lee and K. J. Lee, *Appl. Phys. Lett.*, 2012, **101**, 22405.
14 K. W. Kim, S. M. Seo, J. Ryu, K. J. Lee and H. W. Lee, *Phys. Rev. B: Condens. Matter Mater. Phys.*, 2012, **85**, 180404.
15 T. Koretsune, N. Nagaosa and R. Arita, *Sci. Rep.*, 2015, **5**, 13302.
16 N. H. Kim, D. S. Han, J. Jung, J. Cho, J. S. Kim, H. J. M. Swagten and C. Y. You, *Appl. Phys. Lett.*, 2015, **107**, 142408.
17 A. Hrabec, N. A. Porter, A. Wells, M. J. Benitez, G. Burnell, S. McVitie, D. McGrouther, T. A. Moore and C. H. Marrows, *Phys. Rev. B: Condens. Matter Mater. Phys.*, 2014, **90**, 20402.
18 S. S. P. Parkin, M. Hayashi and L. Thomas, *Science*, 2008, **320**, 190–194.
19 A. Fert, N. Reyren and V. Cros, *Nat. Rev. Mater.*, 2017, **2**, 17031.
20 Y. Sun, Y. Ba, A. Chen, W. He, W. Wang, X. Zheng, L. Zou, Y. Zhang, Q. Yang, L. Yan, C. Feng, Q. Zhang, J. Cai, W. Wu, M. Liu, L. Gu, Z. Cheng, C. W. Nan, Z. Qiu, Y. Wu, J. Li and Y. Zhao, *ACS Appl. Mater. Interfaces*, 2017, **9**, 10855–10864.
21 M. T. Johnson, P. J. H. Bloemen, F. J. A. den Broeder and J. J. de Vries, *Rep. Prog. Phys.*, 1996, **59**, 1409–1458.
22 K. Yakushiji, H. Kubota, A. Fukushima and S. Yuasa, *Appl. Phys. Express*, 2016, **9**, 13003.
23 S. Lemerle, J. Ferré, C. Chappert, V. Mathet, T. Giamarchi and P. Le Doussal, *Phys. Rev. Lett.*, 1998, **80**, 849–852.
24 P. Chauve, T. Giamarchi and P. Le Doussal, *Phys. Rev. B: Condens. Matter Mater. Phys.*, 2000, **62**, 6241–6267.
25 S. Jaiswal, K. Litzius, J. Langer, G. Jakob, B. Ocker, M. Kläui, J. G. Universität-mainz, I. Physik, S. T. Ag and K. Main, *Appl. Phys. Lett.*, 2017, **111**, 42406.
26 A. Thiaville, S. Rohart, E. Jue, V. Cros and A. Fert, *Europhys. Lett.*, 2012, **100**, 57002.
27 M. Vanatka, J.-C. Rojas-Sanchez, J. Vogel, M. Bonfim, A. Thiaville and S. Pizzini, *J. Phys.: Condens. Matter*, 2015, **27**, 326002.
28 C. F. Pai, M. Mann, A. J. Tan and G. S. D. Beach, *Phys. Rev. B*, 2016, **93**, 144409.
29 P. J. Metaxas, J. P. Jamet, A. Mougin, M. Cormier, J. Ferré, V. Baltz, B. Rodmacq, B. Dieny and R. L. Stamps, *Phys. Rev. Lett.*, 2007, **99**, 217208.
30 S. G. Je, D. H. Kim, S. C. Yoo, B. C. Min, K. J. Lee and S. B. Choe, *Phys. Rev. B: Condens. Matter Mater. Phys.*, 2013, **88**, 214401.
31 O. Boulle, J. Vogel, H. Yang, S. Pizzini, D. de S. Chaves, A. Locatelli, T. O. Menteș, A. Sala, L. D. Buda-Prejbeanu, O. Klein, M. Belmeguenai, Y. Roussigné, A. Stashkevich, S. M. Chérif, L. Aballe, M. Föerster, M. Chshiev, S. Auffret, I. M. Miron and G. Gaudin, *Nat. Nanotechnol.*, 2016, **11**, 449–455.
32 R. Lo Conte, G. V. Karnad, E. Martinez, K. Lee, N. H. Kim, D. S. Han, J. S. Kim, S. Prenzel, T. Schulz, C. Y. You, H. J. M. Swagten and M. Kläui, *AIP Adv.*, 2017, **7**, 65317.
33 G. Yu, Z. Wang, M. Abolfath-beygi, C. He, X. Li, K. L. Wong, P. Nordeen, G. P. Carman, X. Han, I. A. Alhomoudi, P. K. Amiri, K. L. Wang, G. Yu, Z. Wang, M. Abolfath-beygi, C. He, X. Li, I. A. Alhomoudi, P. K. Amiri and K. L. Wang, *Appl. Phys. Lett.*, 2015, **106**, 72402.
34 P. V. Ong, N. Kioussis, P. K. Amiri, K. L. Wang, G. P. Carman, P. V. Ong, N. Kioussis, P. K. Amiri, K. L. Wang and G. P. Carman, *J. Appl. Phys.*, 2015, **117**, 17B518.
35 A. Belabbes, G. Bihlmayer, S. Blügel and A. Manchon, *Sci. Rep.*, 2016, **6**, 24634.
36 H. Yang, O. Boulle, V. Cros, A. Fert and M. Chshiev, *arXiv:1603.01847v2*, DOI:DOI: 10.1021/acs.nanolett.5b03392.
37 K. W. Kim, H. W. Lee, K. J. Lee and M. D. Stiles, *Phys. Rev. Lett.*, 2013, **111**, 216601.
38 A. Kundu and S. Zhang, *Phys. Rev. B: Condens. Matter Mater. Phys.*, 2015, **92**, 94434.
39 H. Imamura, P. Bruno and Y. Utsumi, *Phys. Rev. B: Condens. Matter Mater. Phys.*, 2004, **69**, 121303.
40 Y. Gao, Z. Wang, X. Lin, W. Kang, Y. Zhang and W. Zhao, *IEEE Trans. Nanotechnol.*, 2017, **16**, 1138–1142.
41 C. P. Chui and Y. Zhou, *AIP Adv.*, 2015, **5**, 97126.
42 C. Hanneken, F. Otte, A. Kubetzka, B. Dupé, N. Romming, K. von Bergmann, R. Wiesendanger and S. Heinze, *Nat. Nanotechnol.*, 2015, **10**, 1039–1042.
43 Y. Huang, W. Kang, X. Zhang, Y. Zhou and W. Zhao, *Nanotechnology*, 2016, **28**, 08LT02.
44 Y. Zhang, X. Lin, J. P. Adam, G. Agnus, W. Kang, W. Cai, J. R. Coudevylle, N. Isac, J. Yang, H. Yang, K. Cao, H. Cui, D. Zhang, Y. Zhang, C. Zhao, W. Zhao and D. Ravelosona, *Adv. Electron. Mater.*, 2018, **4**, 1700461.